Temperature Dependence and Deuterium Kinetic Isotope Effects in the CH (CD) + C_2H_4 (C_2D_4) Reaction between 295 and 726 K

Holger Thiesemann,[†] Eileen P. Clifford,[‡] Craig A. Taatjes,* and Stephen J. Klippenstein*

Combustion Research Facility, Mail Stop 9055, Sandia National Laboratories, Livermore, California 94551-0969

Received: December 20, 2000; In Final Form: March 28, 2001

Absolute rate coefficients for the reactions CH + C_2H_4 (k_1), CD + C_2H_4 (k_2), CH + C_2D_4 (k_3), and CD + C_2D_4 (k_4) have been measured by the laser photolysis/CW laser-induced fluorescence method at temperatures from 295 to 726 K. The individual rate coefficients can be described by $k_1 = (2.85 \pm 0.02)\ (T/293)^{-(0.31 \pm 0.02)} \times 10^{-10}$ cm^3 molecule^{-1} s^{-1}, $k_2 = (2.40 \pm 0.01)\ (T/293)^{-(0.28 \pm 0.01)} \times 10^{-10}$ cm^3 molecule^{-1} s^{-1}, $k_3 = (2.61 \pm 0.01)\ (T/293)^{-(0.34 \pm 0.01)} \times 10^{-10}$ cm^3 molecule^{-1} s^{-1}, $k_4 = (2.22 \pm 0.01)\ (T/293)^{-(0.21 \pm 0.02)} \times 10^{-10}$ cm^3 molecule^{-1} s^{-1}, where the error estimates are $\pm 2\sigma$ and reflect the precision of the fit. The slight negative temperature dependence is in good agreement with previous determinations of this reaction, and is consistent with barrierless formation of an excited C_3H_5 adduct followed by rapid decomposition. The kinetic isotope effect for deuteration of the CH radical is $k_1/k_2 = 1.19 \pm 0.04$ at room temperature, and declines somewhat with temperature. The kinetic isotope effect for deuteration of the ethylene is $k_1/k_3 = 1.08 \pm 0.04$ at 290 K, and is approximately independent of temperature over the range studied. Quantum chemical calculations of the reaction path indicate that the reaction is dominated by addition, with a minor role possible for insertion.

Introduction

In combustion systems, reactions of CH with small hydrocarbons play a role in the creation of higher hydrocarbons, and hence in the formation of soot. These reactions generally proceed by addition or insertion to form an energized hydrocarbon radical adduct which promptly decomposes by C−H bond fission.[1] The overall reaction is thus addition of one carbon atom to the hydrocarbon molecule. The kinetics of CH reactions with a number of hydrocarbon species have been investigated by several groups.[2−5] The reactions in general display a large rate coefficient and a negative temperature dependence, which is consistent with a mechanism whereby barrierless formation of the radical adduct is the rate-limiting step and subsequent decomposition is rapid. The rate coefficient for the reaction is then equivalent to the high-pressure limit of the adduct formation reaction.[6] Such reactions are sometimes termed capture-limited reactions, a designation that suggests dominance of long-range forces in determining the reaction rate.

The kinetics of barrierless addition reactions are commonly treated theoretically by a variationally corrected transition state theory.[6−10] In principle the location of the transition state is determined by minimizing the reactive flux at different positions along the reaction coordinate. Improved results can be obtained by additionally minimizing the flux relative to variations in the reaction coordinate definition, equivalent to changing the shape of the dividing surface between reactants and products.[11−15] Calculation of frequencies in the transition state region for a barrierless addition requires calculation of a significant part of the reaction path at long intermolecular separations. As a result, treatments where the frequencies of the conserved modes are taken to be invariant are extensively used. This approximation of constant conserved-mode frequencies can be called the "loose transition state" assumption. Often hindered rotor models are applied to the transitional modes.[16−21] These treatments have been moderately successful in modeling the rate coefficients of barrierless addition reactions.

The interpretation of kinetic isotope effects in barrierless reactions must include isotopic differences in the variationally determined transition state, which prevents a simple and general correlation between isotope effects and frequency changes in the transition state. However, in certain cases, assuming invariant conserved-mode frequencies in a canonical or energy-resolved microcanonical variational transition state theory treatment, with the center-of-mass separation as the reaction coordinate, gives simple predictions for kinetic isotope effects. For isotopic substitutions which preserve the location of the center of mass (e.g., $C_2H_4 \rightarrow C_2D_4$), these assumptions yield a kinetic isotope effect equal to the ratio of collision frequencies, regardless of the interaction potential.[22] Larger kinetic isotope effects must arise from variation of the form of the transition state dividing surface (e.g., a variable reaction coordinate) or of a change in the frequencies of the conserved modes between reactants and transition state (i.e., inapplicability of the loose transition state assumption).

In our group we have recently undertaken measurements of deuterium kinetic isotope effects in several barrierless CH reactions.[5,23−25] The kinetic isotope effect forms a complementary constraint to rate coefficient measurements for any transition state theory treatment of a chemical reaction, since the rate coefficient is dominated by low-frequency vibrations in the transition state, while the kinetic isotope effect tends to be governed by changes in the high-frequency modes.[26−28] As a result, the isotope effect may be an indicator of the applicability of loose transition state models, since the high frequency modes

* Authors to whom correspondence should be addressed.
[†] Permanent address: University of Kiel, Institute for Physical Chemistry, Ludewig-Meyn-Str. 8, D-24118 Kiel, Germany.
[‡] Present address: Therma-Wave Inc., 1250 Reliance Way, Fremont, CA 94539.

10.1021/jp0045641 CCC: $20.00
Published on Web 05/11/2001

are generally the conserved modes in the reaction. The reaction of C_2H with O_2 displays a negligible deuterium kinetic isotope effect, as expected from a simple loose transition state theory treatment.[29] However, in several CH reactions (CH + O_2, CH_4, C_2H_2) a significant isotope effect has been measured for deuteration of the radical.[5,23] Most tellingly, deuteration of the hydrocarbon reactant in the CH + CH_4 and CH + C_2H_2 reactions have markedly different effects. Deuteration of the acetylene in the CH + C_2H_2 reaction, which proceeds by barrierless addition, has a negligible effect on the reaction rate coefficient.[5] In the reaction of CH with methane, where formation of an excited ethyl radical adduct must proceed by insertion, the reaction with CD_4 is 40−60% slower than that with CH_4.[3,5] The contrast between the methane and acetylene reactions suggests that the kinetic isotope effect for deuteration of the hydrocarbon may be sensitive to the participation of the substituted C−H bond in the initial adduct formation.

The reaction of CH with ethylene can proceed either by insertion to form an excited allyl radical or by addition to the C═C bond to form a cyclopropyl radical. Recent ab initio calculations have determined that the insertion is energetically accessible;[30] since this mechanism forms the more stable C_3H_5 isomer, it may be a significant contributor to the reaction. The present work determines the absolute rate coefficients, the pressure, and temperature dependence of the following chemical reactions:

$$\mathrm{CH}\ [^2\Pi] + \mathrm{C_2H_4} \rightarrow \text{products} \quad (1)$$

$$\mathrm{CD}\ [^2\Pi] + \mathrm{C_2H_4} \rightarrow \text{products} \quad (2)$$

$$\mathrm{CH}\ [^2\Pi] + \mathrm{C_2D_4} \rightarrow \text{products} \quad (3)$$

$$\mathrm{CD}\ [^2\Pi] + \mathrm{C_2D_4} \rightarrow \text{products} \quad (4)$$

The kinetic isotope effects in the above reactions could differ depending on whether an insertion of the CH radical into the C−H bond of the ethylene or the addition to the C−C double bond is the initial step of the reaction. Additionally, the CH/CD kinetic isotope effect for CH + ethylene can be compared to other reactions of the CH radical. Density functional and QCISD(T) calculations are employed to characterize the reaction path for addition and the saddle point for the insertion channel. Transition state theory calculations using these quantum chemical results suggest that addition dominates the reaction mechanism. The experimental isotope effects are further interpreted in the framework of variational transition state theory.

Experiment

The experiments are performed using the pulsed laser photolysis/continuous wave LIF method. The experimental apparatus has previously been described in detail.[5,24] The CH/CD radicals are produced by multiphoton photolysis of $CHBr_3$/$CDBr_3$ using a focused excimer laser (∼30 mJ/pulse, estimated peak power of ∼6 GW cm^{-2}) at 248 nm. The change of the radical concentration with time is probed by LIF in the (A−X) system using a cw ring dye laser operating near 430 nm. In contrast to earlier experiments where the probe was fiber-coupled into the reaction region, the probe laser beam in the present arrangement is simply telescoped to 5 mm diameter and sent into the reactor directly. The probe is attenuated to less than 3 mW in order to remain in the weak probe limit. The photolysis and probe laser beams cross each other at a right angle, and the fluorescence light is detected perpendicular to both laser beams with a photomultiplier tube operated in single photon counting mode. The photomultiplier output is transferred to a multichannel scaler, where typically 2048 channels with a width of 1.28 μs are accumulated. A chopper in the probe laser beam synchronizes the firing of the excimer laser and the multichannel scaler, while modulating the probe laser beam so that the probe light is present or absent for successive photolysis laser shots. This enables accumulation of the difference of the fluorescence signal with and without probe light, reducing contributions from scattered excimer light and window fluorescence. To achieve a good signal-to-noise ratio the signal is typically added over 2500−6000 laser shots.

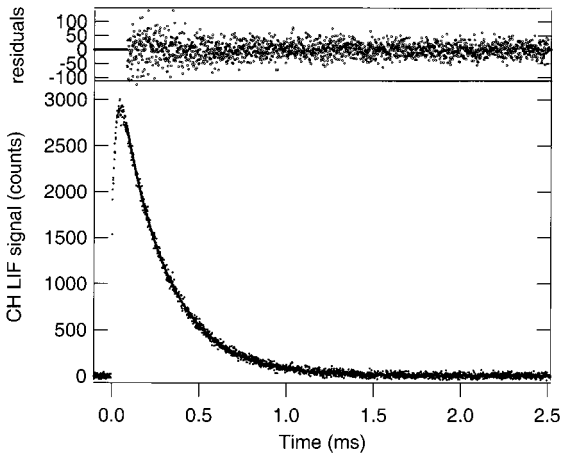

Figure 1. Laser-induced fluorescence signal vs time profile for CD in the reaction CD + C_2H_4, taken at 522.3 K and 100 Torr, with $[C_2H_4] = 4.96 \times 10^{12}$ cm^{-3}. The line in the lower part of the figure shows the result of a single-exponential fit with a decay constant of $\tau = (3870 \pm 20)$ s^{-1}, with the nonweighted residuals displayed above.

The stainless steel reactor can be heated resistively from room temperature up to ∼750 K. The temperature is measured with a thermocouple directly above the observation volume, and the total pressure is monitored by a capacitance manometer. The gas flows are controlled by individually calibrated mass flow meters. To obtain sufficiently small precursor and reactant gas flows, the corresponding compounds were diluted in He and stored in 12 l glass bulbs. Ethylene (C_2H_4, 99.99% and C_2D_4 99 atom % D) were used without further purification; bromoform and $CDBr_3$ were purified by repeated freeze−pump−thaw cycles. The experiments are performed under quasi-static conditions, i.e., the gas flow through the reactor is slow compared to the time scale of the observed chemical reaction but fast enough to prevent a build-up of products in the observation volume.

All reactions were performed under pseudo-first-order conditions, i.e., the reactants were always in great excess over the radical concentration. Each CH/CD decay profile was fitted with a single exponential. A typical concentration time profile is shown in Figure 1 for the reaction of CD with C_2H_4 at 533 K. The observed initial increase of the CD signal corresponds to collisional deactivation of excited states formed in the photolysis. Since the observed vibrational relaxation under the experimental conditions is complete only after at least 10 μs,[31] the earliest data points are ignored during the fitting. The residuals show that the time behavior of the profile is completely described by a single exponential. To extract the second-order rate coefficient the decay constants were plotted against the reactant concentration, as shown in Figure 2. The slope of this plot yields the overall rate coefficient at the respective pressure and temperature, while the intercept reflects loss of CH/CD radicals by reactions with the precursor and possible impurities in the buffer.

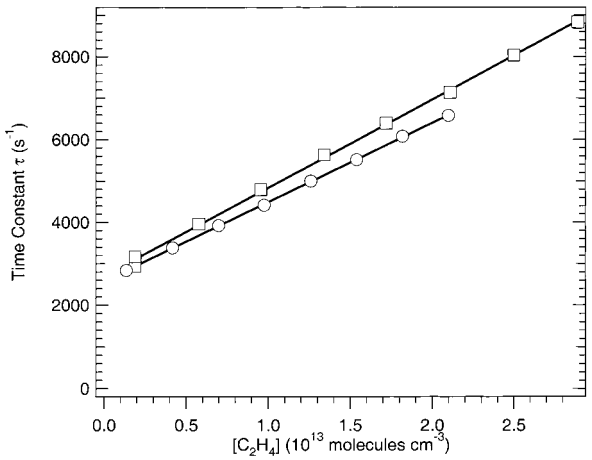

Figure 2. Plot of the first-order decay constant as a function of the reactant concentration for the reactions CD + C_2H_4 (○) and CH + C_2H_4 (□), at $T \sim 725$ K and a total pressure of 100 Torr. Linear fits, shown as the solid lines, yield the second-order rate coefficients. Uncertainties in the precision of the individual time constant determinations are smaller than the symbols used in the plot.

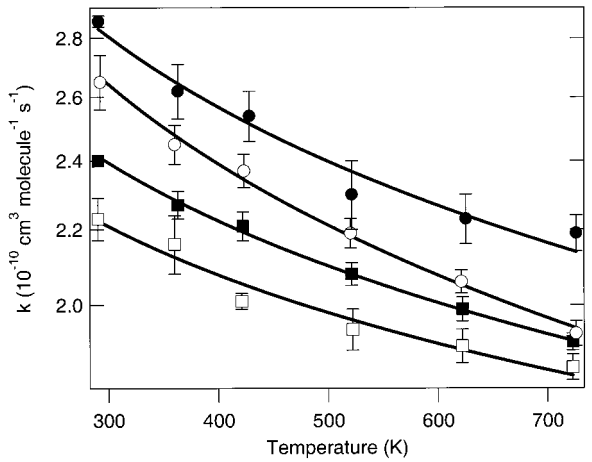

Figure 3. Rate coefficients for reactions 1−4 as a function of temperature: ●, CH + C_2H_4 (k_1); ■, CD + C_2H_4 (k_2); ○, CH + C_2D_4 (k_3); □, CD + C_2D_4 (k_4). Error bars ($\pm 2\sigma$) represent the precision of the individual determinations. The solid lines are fits to an $A\,(T/293)^{-n}$ form, given in Table 1.

Results

Rate coefficients for reactions 1−4 are shown in Figure 3 and summarized in Tables 1 and 2. The room temperature (295 K) rate coefficient for reaction 1 is $(2.86 \pm 0.02) \times 10^{-10}$ cm^3 molecule^{-1} s^{-1}, where the uncertainty represents the statistical error (2σ). Propagation of uncertainties in measurements of temperature, gas composition and pressure leads to an accuracy estimate of ±4%. The rate coefficient is independent of the pressure in the range 15−200 Torr and decreases with increasing temperature (290 K ≤ T ≤ 726 K), as can be seen in Figure 3. The negative temperature dependence is found for all deuterated species as well. A fit to a simple $A\,(T/293)^{-n}$ function gives a comparable small n of 0.2−0.3, as shown in Table 1.

The rate coefficient for the reaction of CH radicals with ethylene found here is in relatively good agreement with the most recent literature values. The earliest published direct measurement of this rate coefficient, from a pulsed radiolysis/VIS absorption experiment reported $k_1 = (1.1 \pm 0.1) \times 10^{-10}$ cm^3 molecule^{-1} s^{-1}.[32] In pulsed laser photolysis/pulsed LIF experiments by Lin and co-workers a room-temperature rate coefficient of $k_1 = (4.2 \pm 0.3) \times 10^{-10}$ cm^3 molecule^{-1} s^{-1} was reported[2] (superseding earlier measurements which gave $k_1 = (2.1 \pm 0.8) \times 10^{-10}$ cm^3 molecule^{-1} s^{-1}, but which suffered from photolysis of the ethylene reactant).[33] Taking the experimental uncertainty into account, our room-temperature rate coefficient of $(2.86 \pm 0.02) \times 10^{-10}$ cm^3 molecule^{-1} s^{-1} is identical to the most recently published laser photolysis/pulsed LIF experiment of Canosa et al. ($(2.9 \pm 0.2) \times 10^{-10}$ cm^3 molecule^{-1} s^{-1}),[4] but is slightly below the Lin measurements.

The present results as well as the previous temperature-dependent determinations of k_1 are shown in Figure 4. The temperature range of the present experiments overlaps with that of Berman et al.,[2] who fitted their data to an Arrhenius expression giving a negative activation energy $E_a/R = (-170 \pm 40)$ K. This in reasonable agreement with a fit to the present results, which yields $E_a/R = (-130 \pm 8)$ K. However, as can be seen from Figure 4, the fitted slope in the previous work is strongly influenced by the data point at the lowest temperature; over the common temperature range the present temperature dependence is in essentially complete agreement with that of Berman et al.

Deuteration at any site reduces the rate coefficient, that is, all kinetic isotope effects are normal. Deuteration of the radical results in a larger kinetic isotope effect than deuteration of the ethylene. For example, at room temperature $k_1/k_2 = 1.19 \pm 0.02$, and $k_1/k_3 = 1.08 \pm 0.09$. Figure 5 shows the average CH/CD and C_2H_4/C_2D_4 kinetic isotope effects over the observed temperature range.

TABLE 1: Parametrization ($k = A\,(T/293)^{-n}$) of Rate Coefficients for the Reactions of CH + C_2H_4 and Isotopic Variants. Error Bars ($\pm 2\sigma$) Represent the Precision of the Fit to the Functional Form

reaction	A [10^{-10} cm^3 molecule^{-1} s^{-1}]	n
CH + C_2H_4 (k_1)	2.85 ± 0.02	0.31 ± 0.02
CD + C_2H_4 (k_2)	2.40 ± 0.01	0.28 ± 0.01
CH + C_2D_4 (k_3)	2.61 ± 0.01	0.34 ± 0.01
CD + C_2D_4 (k_4)	2.22 ± 0.01	0.21 ± 0.02

TABLE 2: Rate Coefficients for the Reactions of CH + C_2H_4 and Isotopic Variants. Error Bars ($\pm 2\sigma$) Represent the Precision of the Individual Determinations

reaction	T [K]	p [Torr]	k [10^{-10} cm^3 molecule^{-1} s^{-1}]
CH + C_2H_4 (k_1)	295	15	2.96 ± 0.04
	295	30	3.0 ± 0.2
	295	75	2.9 ± 0.1
	295	100	2.86 ± 0.02
	295	200	3.1 ± 0.1
	290	100	2.86 ± 0.02
	363	100	2.62 ± 0.09
	428	100	2.54 ± 0.08
	521	100	2.30 ± 0.01
	625	100	2.23 ± 0.07
	726	100	2.19 ± 0.05
CD + C_2H_4 (k_2)	290	100	2.4 ± 0.1
	363	100	2.27 ± 0.04
	422	100	2.21 ± 0.04
	521	100	2.08 ± 0.03
	622	100	1.99 ± 0.03
	723	100	1.91 ± 0.02
CH + C_2D_4 (k_3)	292	100	2.65 ± 0.09
	360	100	2.45 ± 0.06
	423	100	2.37 ± 0.05
	520	100	2.19 ± 0.04
	621	100	2.06 ± 0.03
	726	100	1.93 ± 0.03
CD + C_2D_4 (k_4)	290	100	2.23 ± 0.06
	360	100	2.16 ± 0.08
	421	100	2.01 ± 0.02
	522	100	1.94 ± 0.05
	622	100	1.90 ± 0.04
	723	100	1.85 ± 0.03

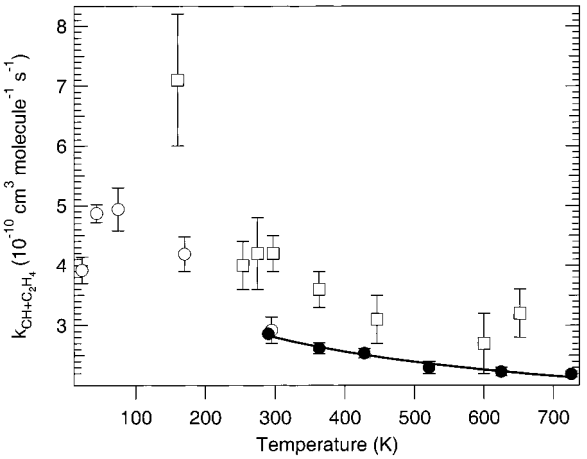

Figure 4. Temperature dependence of the rate coefficient for CH + C_2H_4 (k_1). Present results are shown as the filled circles (●). Results from ref 4 and ref 2 are shown as open circles (○) and open squares (□), respectively.

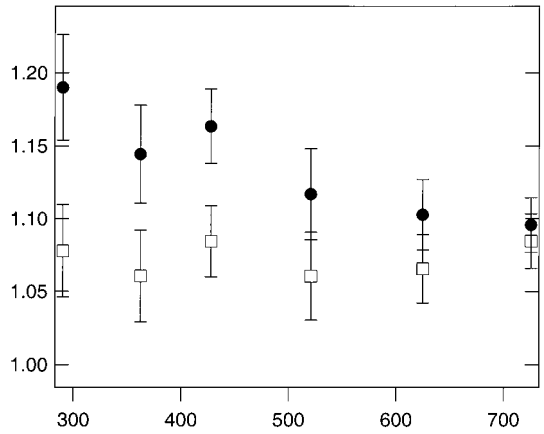

Figure 5. Kinetic isotope effects in the CH + ethylene reaction. The average kinetic isotope effect for deuteration of the CH radical, $(k_1 + k_3)/(k_2 + k_4) = (k_{CH+C_2H_4} + k_{CH+C_2D_4})/(k_{CD+C_2H_4} + k_{CD+C_2D_4})$, is shown as the filled circles (●) and the average kinetic isotope effect for deuteration of the ethylene, $(k_1 + k_2)/(k_3 + k_4) = (k_{CH+C_2H_4} + k_{CD+C_2H_4})/(k_{CH+C_2D_4} + k_{CD+C_2D_4})$, as the open squares (□). The error bars represent $\pm 2\sigma$ uncertainty estimates.

$$\frac{\overline{k_{CH}}}{k_{CD}} \equiv \frac{(k_{CH+C_2H_4} + k_{CH+C_2D_4})}{(k_{CD+C_2H_4} + k_{CD+C_2D_4})} \quad (5)$$

$$\frac{\overline{k_{C_2H_4}}}{k_{C_2D_4}} \equiv \frac{(k_{CH+C_2H_4} + k_{CD+C_2H_4})}{(k_{CH+C_2D_4} + k_{CD+C_2D_4})} \quad (6)$$

The kinetic isotope effect for deuteration of the radical decreases with increasing temperature, while the smaller kinetic isotope effect for deuteration of ethylene is roughly constant with temperature.

To our knowledge there has been no previous determination of the kinetic isotope effect of the CH + C_2H_4 reaction, but it can be compared to the kinetic isotope effect of the reaction CH + CH_4 and CH + C_2H_2.[5] The CH/CD kinetic isotope effect for CH + ethylene, $(k_1 + k_3)/(k_2 + k_4)$ is 1.19 ± 0.04 at room-temperature decreasing to 1.10 ± 0.02 at 720 K. By comparison, the ratio of the collision frequencies of the isotopic labeled species is $k_1/k_2 = 1.03$ and $k_1/k_3 = 1.02$, respectively. Kinetic isotope effects of similar magnitude and temperature dependence have been found in the reactions of CH/CD with O_2,[23] methane, and acetylene.[5] However these reactions show different kinetic isotope effects for deuteration of the hydrocarbon reactant, which is at most weakly dependent on the temperature. The kinetic isotope effect in the reaction of CH with methane is considerably larger $((k_{CH+CH_4} + k_{CD+CH_4})/(k_{CH+CD_4} + k_{CD+CD_4}) = 1.59 \pm 0.09$ at 290 K)[5] than in the reaction with ethylene ($C_2H_4/C_2D_4 = (k_1 + k_2)/(k_3 + k_4) = 1.08 \pm 0.03$ at 295 K), whereas deuteration of acetylene results in no change of the rate coefficient.[5]

Theoretical Investigation of Addition versus Insertion in CH + C_2H_4

It is interesting to consider from a theoretical perspective the relative contributions from the addition and insertion paths, particularly since the two paths might be expected to have significantly different kinetic isotope effects. The insertion path leads directly to the allyl radical, while the addition path leads initially to the cyclopropyl radical. However, at the chemically activated energies arising from the CH + C_2H_4 addition, the cyclopropyl radical will rapidly isomerize to the allyl radical. In the absence of rapid collisional stabilization, the allyl radical will dissociate into allene + H, which is substantially exothermic relative to CH + C_2H_4. In any case, both paths would generally lead to the same products.

Prior theoretical studies suggest that the addition path is barrierless with no saddlepoint to the formation of the cyclopropyl radical.[30,34] For the insertion path, there is some uncertainty as to the presence or absence of a saddlepoint. An endothermic saddlepoint was found in both CISD/ROHF[34] and CASSCF[30] calculations. However, Wang and Huang were unable to find a saddlepoint at the MP2 level, even when making use of the information from the CASSCF transition state.[30]

The reaction path energetics for these two channels are reanalyzed here with a combination of density functional theory optimizations and QCISD(T) calculations with the ultimate aim of obtaining some reasonably reliable indication of the relative contributions of the two channels. First, the B3LYP density functional is employed in optimizations along the reaction paths using the 6-31G** basis set. Then B3LYP and QCISD(T) calculations employing the 6-311++G** basis set, and MP2 calculations employing the 6-311++G(*3df,2pd*) basis are performed at these reaction path geometries. These calculations yield approximate QCISD(T)/6-311++G(*3df,2pd*) energies via the relation:

$$\text{QCISD(T)/6-311++G(}3df,2pd\text{)} \sim \text{QCISD(T)/6-311++G**} + \text{MP2/6-311++G(}3df,2pd\text{)} - \text{MP2/6-311++G**}$$

The present computations employed the Gaussian98 software.[35]

The calculated reaction path energetics for the addition channel are illustrated in Figure 6, as a function of the distance R_{CX} between the CH carbon and the midpoint of the line containing the two ethylene carbons. The CH radical is constrained to lie in the C_s symmetry plane in these addition path optimizations and the CH is thus more or less perpendicular to the C═C bond in this path. The three results are reasonably similar and clearly indicate a strongly attractive reaction path with no barrier to the simple addition reaction.

A saddlepoint for the insertion process was found at the B3LYP/6-31G** level, which after zero-point corrections was 1.95 and 3.74 kcal/mol below reactants for the QCISD(T)/6-311++G(*3df,2pd*) and B3LYP/6-311++G** calculations, respectively. A contour plot illustrating the variation in the

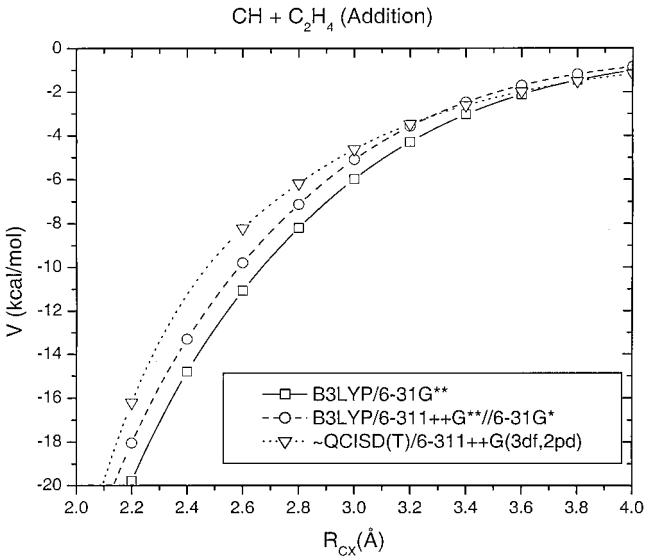

Figure 6. Calculated reaction path energies for the addition of CH + C_2H_4 to form an excited cyclopropyl radical.

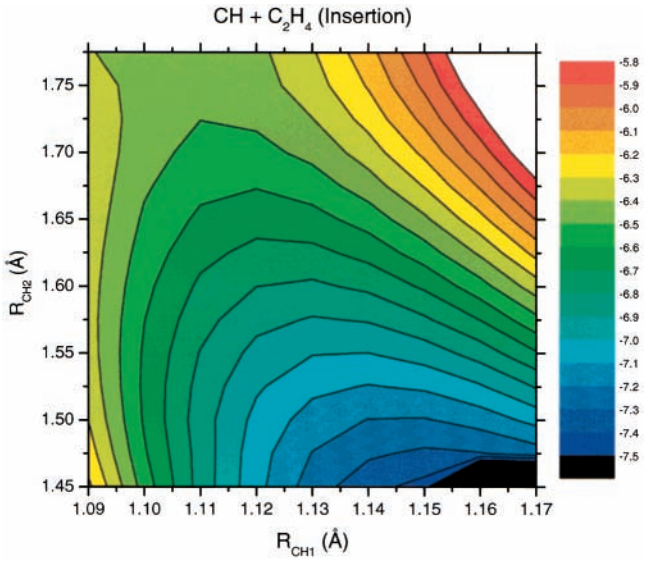

Figure 7. Contour plot of the potential energy variation in the region of the insertion saddlepoint, calculated at the B3LYP/6-31G** level. R_{CH1} refers to the length of the ethylene C−H bond where the insertion occurs, and R_{CH2} is the distance from the carbon atom in the approaching CH radical to the H atom in the same ethylene C−H bond.

B3LYP/6-31G** potential in the neighborhood of the saddlepoint (not including zero-point energy) is provided in Figure 7. The coordinates R_{CH1} and R_{CH2} in this plot correspond to the CH distance for the bond in ethylene where the insertion is occurring, and the distance from the H atom in that bond to the C atom of the incoming CH fragment. All other coordinates in this plot were allowed to fully relax.

One notable aspect of this plot is the minimal variation in the potential from the saddlepoint (at the top left) where the incoming CH is still quite distant from the CH in ethylene, to the bottom right where the incoming CH is now quite close to the ethylene CH and the latter CH bond is rapidly extending. The one-dimensional plot of the calculated energetics along the reaction path, provided in Figure 8, further illustrates this slow variation of the reaction path energy. The numbers plotted there are all relative to infinitely separated reactants and do not include a zero-point correction, in contrast with the numbers reported above for the saddlepoint energies.

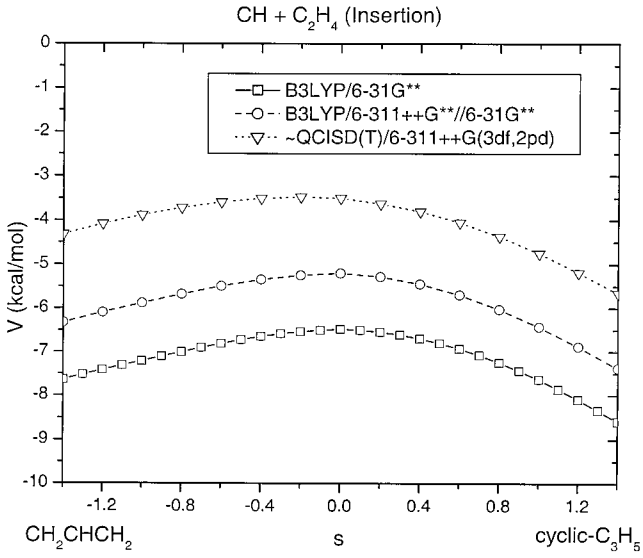

Figure 8. Reaction path energies for the insertion pathway of CH + C_2H_4 to form an excited allyl radical. The reaction coordinate *s* for these plots is that obtained from an intrinsic reaction coordinate calculation with negative values corresponding to the effective motion toward allyl radical and positive values corresponding to the effective motion toward cyclopropyl radical. The latter motion initially appears to be toward CH + C_2H_4, but ultimately finds its way into the addition well corresponding to cyclopropyl radical.

Interestingly, the B3LYP/6-31G** saddlepoint geometry differs greatly from that reported in ref 30. In particular, at the CASSCF(7,8)/6-31G** level R_{CH1} and R_{CH2} are reported to be 1.249 and 1.269 Å, respectively, while the present B3LYP/6-31G** values are 1.758 and 1.109 Å, respectively. The combination of this large scale difference in the geometries, the flat nature of the potential, and the presence of significant spin contamination at the MP2 level are likely related to the difficulty of locating the saddlepoint at the MP2/6-31G** level.

A comparison of the reaction path energies for the addition and insertion pathways is useful in assessing, if only qualitatively, the likely branching between insertion and addition. The CC separation at the insertion saddlepoint is only 2.308 Å. At the equivalent R_{CX} value the addition path is already about 15 kcal mol^{-1} attractive. Past experience suggests that for reasonable temperatures the transition state for the addition path will lie at larger separations where the maximum attractiveness is significantly smaller. To verify this sample variational transition state theory (VTST) calculations were performed. These VTST calculations employed a simple model potential for the transitional modes based on fits of sinusoidally hindered forms to the B3LYP/6-31G** calculated quadratic force field along the reaction path. A more detailed description of such hindered rotor potentials is provided in ref 36. The present potential form for the hindering motion differs only in the use of interpolations in place of extrapolations, and in the use of a three term Fourier fit [$V = V_0 + V_1 \cos(2\theta_{CXC}) + V_2 \cos(4\theta_{CXC})$] for the potential in the CXC angle (where X is the midpoint of the CC bond in C_2H_4).

The rate constants resulting from *E*/*J* resolved minimization with a reaction coordinate defined by the C (of CH) to CC midpoint separation are plotted in Figure 9 and shown in Table 3. Reaction coordinate values ranging from 2.0 to 3.8 Å were considered in the analysis. Larger separations were not considered due to limitations in the method for generating the reference force field. As a result, calculations were not performed for temperatures lower than 300 K, since the transition state then lies at too large a separation. In fact, the neglect of the large

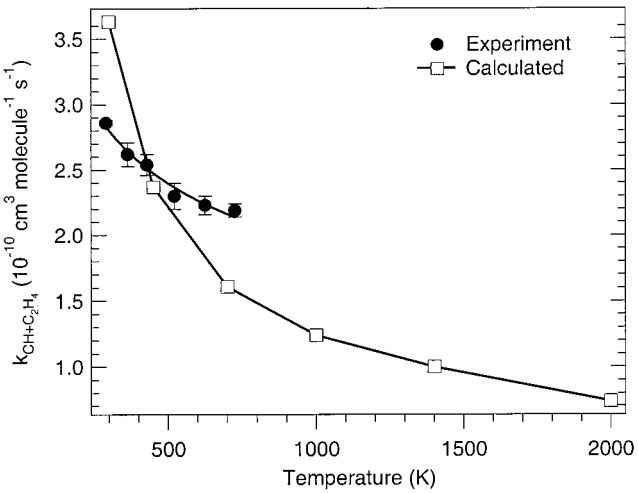

Figure 9. Comparison of experimental rate coefficients (●) with results of *E*/*J*-resolved variational transition state theory calculations (□).

TABLE 3: *E*/*J*-resolved VTST Calculated Rate Coefficients for the Reaction of CH + C_2H_4

T [K]	rate coefficient
300	3.63×10^{-10} cm^3 molecule^{-1} s^{-1}
450	2.37×10^{-10} cm^3 molecule^{-1} s^{-1}
700	1.61×10^{-10} cm^3 molecule^{-1} s^{-1}
1000	1.24×10^{-10} cm^3 molecule^{-1} s^{-1}
1400	1.00×10^{-10} cm^3 molecule^{-1} s^{-1}
2000	7.41×10^{-11} cm^3 molecule^{-1} s^{-1}

separation values may be related to the too sharp decrease with temperature of the predicted rate constants. The calculated transition state separations range from about 3.6 Å near room temperature to about 2.6 Å near 2000 K. At 800 K, the transition state lies at CC separations of about 2.9 Å, whereas the transition state partition function at a separation of 2.3 Å is a factor of 4 greater.

These sample calculations for the addition path indicate that the insertion saddlepoint is located considerably closer in than the bottleneck for the addition. In fact, reaction path following from the insertion saddle point actually leads directly to the cyclopropyl complex rather than the CH + C_2H_4 reactants. Clearly, the branching between the insertion and addition reactions is determined separately from the bottleneck for the overall rate, which should correspond simply to the bottleneck for the addition, at least for not too high a temperature.

The ratio of the reactive fluxes for the addition and insertion channels, both at CC separations corresponding to the insertion saddlepoint, should provide a crude estimate for the expected branching ratio. The vibrational frequencies at the insertion saddlepoint were reanalyzed at the B3LYP/6-311++G** level (which yielded essentially no change in geometry). These frequencies were then employed, together with the QCISD(T)/6-311++G(*3df,2pd*) energetic estimates and rigid-rotor harmonic oscillator assumptions, in conventional TST estimates of the rate constants for the various isotopically substituted insertion reactions. The resulting predictions for the temperature dependence of the rate constants and kinetic isotopic effects (when considering only this insertion saddlepoint) are illustrated in Figures 10 and 11, respectively.

The negative energy for the insertion saddlepoint implies that at low enough temperatures the saddlepoint does not provide the dominant bottleneck to reaction, as discussed above. Furthermore, at high temperatures, the insertion bottleneck will likely move in to shorter separations than that of the saddlepoint, to reduce the entropy of the transition state. As a result, the

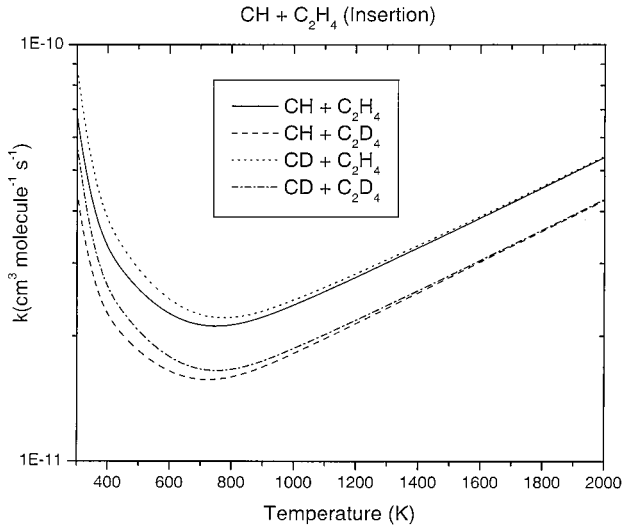

Figure 10. Transition state theory estimates for the rate coefficient of insertion, based on the B3LYP/6-311++G** vibrational frequencies and the QCISD(T)/6-311++G(*3df,2pd*) energies.

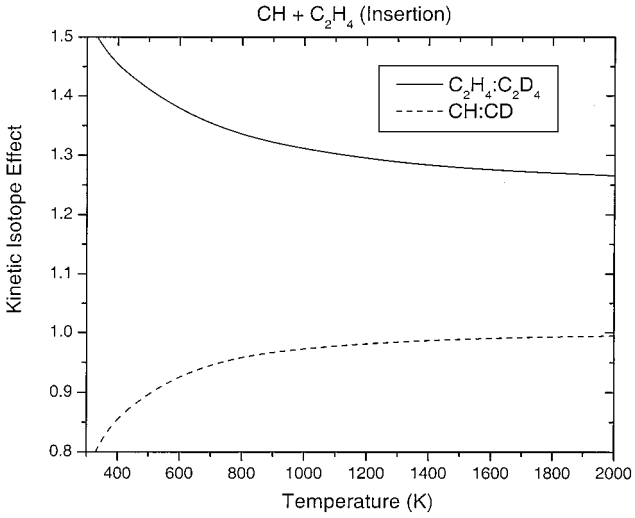

Figure 11. Transition state theory estimates for the kinetic isotope effects in the insertion channel, based on the B3LYP/6-311++G** vibrational frequencies and the QCISD(T)/6-311++G(*3df,2pd*) energies.

region where the calculated rate constants are most likely to be semiquantitatively correct is where they approach their minimum value, i.e., near 800 K. At 800 K, this insertion rate constant is about a factor of 8 lower than the experimental rate, suggesting a maximum contribution of about 12% for the insertion channel.

A more appropriate estimate of the branching ratio is probably obtained by comparing the reactive flux through this insertion saddlepoint with the corresponding reactive flux for the addition channel at the same separation. This ratio is smaller than the ratio of reactive fluxes calculated above, being less than 0.01 for temperatures lower than 500 K, but does gradually increase with temperature. At 700, 1000, 1400, and 2000 K it is about 0.02, 0.06, 0.15, and 0.4, respectively. The increase in the insertion rate, and thus the branching ratio, at the highest temperatures is probably artificial, as the insertion transition state likely moves to closer CC separations as the temperature increases, with a concomitant decrease in the predicted insertion rate constant.

Qualitatively similar results, but with the insertion contribution increased by nearly a factor of 3 near 800 K, are obtained when the QCISD(T)/6-311++G(*3df,2pd*) estimate of the sad-

dlepoint energy is replaced with the B3LYP/6-311++G** estimate. Thus, the calculations suggest that the branching through the insertion channel is likely about 10% or less of the total reactive flux.

Discussion

Thermal rate coefficient measurements provide an important avenue to understanding the mechanism of chemical reactions, but in translating the experimental observations into a theoretical grasp of the fundamental chemistry, one is often simply reduced to a call for more accurate potential energy surfaces. Isotopic substitution offers a means to focus on selected aspects of the reaction which are often complementary to those probed by total rate coefficient measurements. The interpretation of kinetic isotope effects is generally based on transition state theory.[7] The kinetic behavior of the CH + ethylene reaction can be described as a barrierless recombination reaction, which has no single well-defined transition state geometry. Transition state theory descriptions of reactions occurring without a potential barrier require a variational determination of the transition state configuration, typically relying on a separation between the conserved modes of the system, i.e., those modes which correspond to vibrational modes of the separated reactants, and the transitional modes. Measurements of kinetic isotope effects are most affected by high-frequency modes, whereas the total rate coefficient is most sensitive to the low-frequency transitional modes. The kinetic isotope effect measurement may therefore be sensitive to changes in the conserved mode frequencies at the transition state. However, it is useful to first consider the kinetic isotope effects which can arise without conserved frequency variations. A more detailed description of general considerations of kinetic isotope effects and variable reaction coordinates will be the subject of a subsequent paper.

In canonical and, assuming vibrational adiabaticity, in microcanonical formulations of variational transition state theory, use of the center-of-mass separation as the reaction coordinate allows the dependence on the reaction coordinate to be collected in a single factor which depends on the potential in spatial coordinates. The potential energy surface is invariant to isotopic substitution under the Born−Oppenheimer approximation, but the location of the fragment center of mass can be changed by isotopic substitution, which leads to a slightly different configuration integral for the same center-of-mass separation. However, for deuteration of ethylene the position of the center of mass is unchanged by the substitution, and the kinetic isotope effect can be straightforwardly calculated to be the collision frequency ratio regardless of the interaction potential. The kinetic isotope effects observed in the present reactions are larger than can be explained on the basis of variational transition state theory using a loose transition state assumption and the center of mass separation as the reaction coordinate. Therefore, if the reaction is assumed to be describable by a variational transition state theory treatment, either the reaction coordinate differs from the center of mass separation, or the conserved frequencies are not constant during the reaction. (A third possibility is that the rate coefficient may depend markedly on the angular momentum, requiring a *J*-resolved microcanonical variational transition state theory treatment.[37] However, except for ion−molecule reactions the inclusion of such *J*-dependence to the transition states yields reductions of only about 10% for the high pressure thermal rate coefficient.[11,12,38])

Currently the most successful transition state theory treatments of barrierless association reactions employ a reaction coordinate that is allowed to depart from the center of mass separation. Previous work has shown that a redefinition of the reaction coordinate can result in significant reduction of the estimated rate coefficient,[11,12] and methodology for equivalent variational minimization with respect to choice of reaction coordinate has been introduced by several other investigators.[13−15] A generalized variable reaction coordinate can be defined by designating as the reaction coordinate the distance between two fixed points (call them x_1, x_2) in the individual molecular frames, not necessarily located at the centers of mass of the molecules. For example, at small separations, the incipient bond length, i.e., the distance between the centers of the two atoms forming the new bond, may be a natural choice for a reaction coordinate. The coupling of rotational motion to the reaction coordinate can give rise to a kinetic isotope effect.[22]

The moments of inertia of the individual reactants contribute to the function to be minimized only insofar as their corresponding rotations q change the reaction coordinate s, via terms of the form $\partial s/\partial q$.[13,14,39,40] This implies that a moment of inertia in molecule i is only important in the minimization if the fixed point x_i lies off the axis of rotation. For example, if a change in the A rotational constant of the ethylene molecule is to affect the position of the variationally determined transition state, rotation about the C−C bond must change the reaction coordinate, and the fixed point in the ethylene molecule must therefore lie off the C−C axis. The kinetic isotope effect which can be produced from a change in reaction coordinate can be significant; in a separate paper we will present calculations using model potentials that predict CH/CD isotope effects in reasonable conformity with the experimentally observed isotope effects including those of the present study.[22] These results suggest that kinetic isotope effects in barrierless addition reactions are sensitive to the nature of the reaction coordinate.

On the other hand, the isotope effect generated from a change in the conserved mode frequencies can be calculated using the standard expression for a kinetic isotope effect with a fixed transition state,[26,27] which can be simply written by framing the partition function in terms of local properties:[28,41]

$$\frac{k_H}{k_D} = \frac{\nu_H^{\ddagger}}{\nu_D^{\ddagger}} \prod^{3n-6} \left(\frac{\gamma_H}{\gamma_D}\right)^{\ddagger} \cdot \prod \left(\frac{\gamma_D}{\gamma_H}\right)_{\text{reactants}} \tag{7}$$

Here the ν's are vibrational frequencies, with $\nu^{\ddagger}$ the (imaginary) frequency of the reaction coordinate, and the functions γ are quantum corrections to the classical vibrational partition function of the form

$$\gamma = \frac{\frac{u}{2}}{\sinh\left(\frac{u}{2}\right)} \tag{8}$$

with $u = h\nu/kT$. If the observed kinetic isotope effect were to arise from a change in the conserved mode frequency corresponding to the substituted bond, the dominant contribution should be the change in the vibrational partition function, as described by eqs 7 and 8. The contribution resulting from concomitant changes in the moments of inertia will generally be smaller.

The present observations can be interpreted in the light of these possible contributions to kinetic isotope effects in barrierless reactions. First, if the change in reactivity for deuterium substitution of the CH radical in the present study were to be described by a change in the C−H stretching frequency between the reactants and the transition state, the kinetic isotope effect

could be approximated by

$$\frac{k_{CH}}{k_{CD}} \approx \left(\frac{\mu_{CD}}{\mu_{CH}}\right)^{1/2} \left(\frac{\gamma_{CH}}{\gamma_{CD}}\right)^{\ddagger} \left(\frac{\gamma_{CD}}{\gamma_{CH}}\right)_{\text{reactants}} \quad (9)$$

where the only contributing frequency is that of the radical C−H stretch. To produce the observed kinetic isotope effect of ∼1.2, the frequency of the radical C−H stretch would need to decrease by 5−10% between the free molecule and the transition state.[23] A decrease of this magnitude in CH + hydrocarbon reactions seems extremely unlikely based on recent ab initio calculations.[42−45] A variable reaction coordinate transition state theory provides a more plausible explanation for the CH/CD kinetic isotope effect, as will be discussed in detail in a subsequent paper.[22]

Quantum chemical calculations have shown that the transition state for the addition of CH to the double bond of ethylene is comparable to that for CH adding to the triple bond of acetylene.[30,34,44] In both cases the CH attacks the C−C bond, leaving the geometry of the respective hydrocarbon reactant approximately unchanged during the formation of the transition state. Consequently, the parts of the partition functions affected by the isotopic substitution in the ethylene/acetylene should remain unchanged on the part of the reaction path from the reactants to the transition state. On the other hand, the transition states for insertion of CH into hydrocarbons necessarily involve some weakening of the hydrocarbon C−H bond which is attacked, and this decrease in frequency must supply some contribution to the kinetic isotope effect for deuterium substitution on the hydrocarbon reagent.

The predicted isotope effects for the insertion channel (Figure 11) are qualitatively similar to those calculated for the CH + CH_4 reaction. In particular, the CH:CD isotope effect is actually less than unity in contradistinction with the experimental results. This observation, coupled with the smallness of the variation in the conserved mode force field for the addition path, give further indication that the observed CH:CD kinetic isotope effects are due to the particular form of the optimized reaction coordinate.[22] Meanwhile, the C_2H_4:C_2D_4 kinetic isotope effect for the insertion channel is near 1.3 and a small contribution from this channel would help to reproduce the experimental observations.

However, since the isotope effect for deuteration of ethylene is small (smaller than that observed for deuteration of the CH radical), the data cannot be construed as clear evidence for an insertion mechanism. In fact, the present results could be consistent with a pure addition reaction, if the reaction coordinate for the addition is coupled to the *A* rotation of the ethylene molecule. This would correspond to the fixed point for ethylene, x_2 in the generalized reaction coordinate treatment described above, lying away from the C−C axis. A reaction coordinate for addition corresponding to the distance between the radical orbital on the CH and the π orbitals of the ethylene double bond is physically reasonable and could reproduce the experimental results.

Conclusions

The overall rate coefficients for the reactions CH/CD + C_2H_4/C_2D_4 were determined in the pressure range 15 Torr ≤ P ≤ 200 Torr and temperature range 290 K ≤ T ≤ 720 K. The magnitude of the rate coefficients and their negative temperature dependence are typical for barrierless association reactions with subsequent fast decay of the transition complex. The kinetic isotope effect for deuteration of the CH radical (19 ± 4%) is comparable with other association limited CH reactions and can be explained with a variable reaction coordinate that deviates from the center-of-mass separation. The effect of deuteration of ethylene is 8 ± 3%, lying between the isotope effect of the reaction CH + C_2H_2 (0 ± 2%) and CH + CH_4 (60 ± 13%). The kinetic isotope effect for deuteration of the ethylene reagent does not allow a clear experimental differentiation between the competing addition and insertion pathways. The quantum chemical calculations presented here suggest that insertion is a minor channel.

Acknowledgment. This work is supported by the Division of Chemical Sciences, the Office of Basic Energy Sciences, the U.S. Department of Energy. These experiments depended on the expert technical assistance of Leonard Jusinski. H.T. acknowledges the Deutsche Forschungsgemeinschaft (DFG) for a cooperative research grant.

References and Notes

(1) Sanders, W. A.; Lin, M. C. In *Chemical Kinetics of Small Organic Radicals*; Alfassi, Z., Ed.; CRC Press: Boca Raton, FL, 1988; Vol. 3.
(2) Berman, M. R.; Fleming, J. W.; Harvey, A. B.; Lin, M. C. *Chem. Phys.* **1982**, *73*, 27.
(3) Blitz, M. A.; Johnson, D. G.; Pesa, M.; Pilling, M. J.; Robertson, S. H.; Seakins, P. W. *J. Chem. Soc. Faraday Trans.* **1997**, *93*, 1473.
(4) Canosa, A.; Sims, I. R.; Travers, D.; Smith, I. W. M.; Rowe, B. R. *Astron. Astrophys.* **1997**, *323*, 644.
(5) Thiesemann, H.; MacNamara, J.; Taatjes, C. A. *J. Phys. Chem. A* **1997**, *101*, 1881.
(6) Gilbert, R. G.; Smith, S. C. *Theory of Unimolecular and Recombination Reactions*; Blackwell Scientific Publications: Oxford, 1990.
(7) Truhlar, D. G.; Garrett, B. C.; Klippenstein, S. J. *J. Phys. Chem.* **1996**, *100*, 12771.
(8) Robertson, S. H.; Wagner, A. F.; Wardlaw, D. M. *J. Chem. Phys.* **1995**, *103*, 2917.
(9) Holbrook, K. A.; Pilling, M. J.; Robertson, S. H. *Unimolecular Reactions*, 2nd ed.; John Wiley & Sons: Chichester, 1996.
(10) Baer, T.; Hase, W. L. *Unimolecular Reaction Dynamics*; Oxford University Press: Oxford, 1996.
(11) Klippenstein, S. J.; Allen, W. D. *Ber. Bunsen-Ges.. Phys. Chem.* **1997**, *101*, 423.
(12) Klippenstein, S. J. *J. Chem. Phys.* **1991**, *94*, 6469.
(13) Robertson, S. H.; Wagner, A. F.; Wardlaw, D. M. *Faraday Discuss.* **1995**, *102*, 65.
(14) Smith, S. C. *J. Chem. Phys.* **1999**, *111*, 1830.
(15) Smith, S. C. *J. Phys. Chem.* **1994**, *96*, 6496.
(16) Jordan, M. J. T.; Smith, S. C.; Gilbert, R. G. *J. Phys. Chem.* **1991**, *95*, 8685.
(17) Hase, W. L.; Zhu, L. *Int. J. Chem. Kinet.* **1994**, *26*, 407.
(18) Hu, X.; Hase, W. L. *J. Phys. Chem.* **1989**, *93*, 6029.
(19) McClurg, R. B.; Flagan, R. C.; Goddard, W. A., III. *J. Chem. Phys.* **1997**, *106*, 6675.
(20) Pacey, P. D. *J. Phys. Chem. A* **1998**, *102*, 8541.
(21) Wagner, A. F.; Harding, L. B.; Robertson, S. H.; Wardlaw, D. M. *Ber. Bunsen-Ges. Phys. Chem.* **1997**, *101*, 391.
(22) Taatjes, C. A.; Klippenstein, S. J. Submitted.
(23) Taatjes, C. A. *J. Phys. Chem.* **1996**, *100*, 17840.
(24) Taatjes, C. A. *J. Chem. Phys.* **1997**, *106*, 1786.
(25) Taatjes, C. A. *J. Chem. Phys.* **1997**, *107*, 10829.
(26) Melander, L.; Saunders, W. H., Jr. *Reaction Rates of Isotopic Molecules*; John Wiley and Sons: New York, 1980.
(27) VanHook, W. A. In *Isotope Effects in Chemical Reactions*; Collins, C. J., Bowman, N. S., Eds.; Van Nostrand Reinhold: New York, 1970.
(28) Johnston, H. S. *Gas Phase Reaction Rate Theory*; Ronald Press: New York, 1966.
(29) Thiesemann, H.; Taatjes, C. A. *Chem. Phys. Lett.* **1997**, *270*, 580.
(30) Wang, Z.-X.; Huang, M.-B. *Chem. Phys. Lett.* **1998**, *291*, 381.
(31) Blitz, M. A.; Pesa, M.; Pilling, M. J.; Seakins, P. W. *Chem. Phys. Lett.* **2000**, *322*, 280.
(32) Bosnali, M. W.; Perner, D. *Z. Naturforsch.* **1971**, *26A*, 1768.
(33) Butler, J. E.; Fleming, J. W.; Goss, L. P.; Lin, M. C. *Chem. Phys.* **1981**, *56*, 355.
(34) Gosavi, R. K.; Safarik, I.; Strausz, O. P. *Can. J. Chem.* **1985**, *63*, 1689.
(35) Frisch, M. J.; Trucks, G. W.; Schlegel, H. B.; Scuseria, G. E.; Robb, M. A.; Cheeseman, J. R.; Zakrzewski, V. G.; Montgomery, J. A., Jr.; Stratmann, R. E.; Burant, J. C.; Dapprich, S.; Millam, J. M.; Daniels, A.

D.; Kudin, K. N.; Strain, M. C.; Farkas, O.; Tomasi, J.; Barone, V.; Cossi, M.; Cammi, R.; Mennucci, B.; Pomelli, C.; Adamo, C.; Clifford, S.; Ochterski, J.; Petersson, G. A.; Ayala, P. Y.; Cui, Q.; Morokuma, K.; Malick, D. K.; Rabuck, A. D.; Raghavachari, K.; Foresman, J. B.; Cioslowski, J.; Ortiz, J. V.; Stefanov, B. B.; Liu, G.; Liashenko, A.; Piskorz, P.; Komaromi, I.; Gomperts, R.; Martin, R. L.; Fox, D. J.; Keith, T.; Al-Laham, M. A.; Peng, C. Y.; Nanayakkara, A.; Gonzalez, C.; Challacombe, M.; Gill, P. M. W.; Johnson, B.; Chen, W.; Wong, M. W.; Andres, J. L.; Gonzalez, C.; Head-Gordon, M.; Replogle, E. S.; Pople, J. A. *Gaussian 98*; Gaussian, Inc.: Pittsburgh, PA, 1998.

(36) Miller, J. A.; Klippenstein, S. J. *J. Phys. Chem. A* **2000**, *104*, 2061.

(37) Smith, S. C. *J. Chem. Phys.* **1992**, *97*, 2406.

(38) Aubanel, E. E.; Wardlaw, D. M. *Chem. Phys. Lett.* **1990**, *167*, 145.

(39) Robertson, S.; Wagner, A. F.; Wardlaw, D. M. *J. Chem. Phys.* **2000**, *113*, 2648.

(40) Smith, S. C. *J. Phys. Chem. A* **2000**, *104*, 10489.

(41) Herschbach, D. R.; Johnston, H. S.; Rapp, D. *J. Chem. Phys.* **1959**, *31*, 1652.

(42) Vereecken, L.; Peeters, J. *J. Phys. Chem. A* **1999**, *103*, 5523.

(43) Vereecken, L.; Pierloot, K.; Peeters, J. *J. Chem. Phys.* **1998**, *108*, 1068.

(44) Walch, S. P. *J. Chem. Phys.* **1995**, *103*, 7064.

(45) Guadagnini, R.; Schatz, G. C.; Walch, S. P. *J. Phys. Chem. A* **1998**, *102*, 5857.